Published OnlineFirst April 29, 2019; DOI: 10.1158/1541-7786.MCR-18-1361

Cell Fate Decisions

Molecular Cancer Research

Hyperphosphorylation of CDH1 in Glioblastoma Cancer Stem Cells Attenuates APC/C^{CDH1} Activity and Pharmacologic Inhibition of APC/C$^{CDH1/CDC20}$ Compromises Viability

Kuntal De[1], Treg M. Grubb[1], Abigail A. Zalenski[1,2], Kayla E. Pfaff[1,3], Debjani Pal[1], Shubhra Majumder[4], Matthew K. Summers[1], and Monica Venere[1]

Abstract

Glioblastoma (GBM) is the most common and lethal primary brain tumor and remains incurable. This is in part due to the cellular heterogeneity within these tumors, which includes a subpopulation of treatment-resistant cells called cancer stem–like cells (CSC). We previously identified that the anaphase-promoting complex/cylosome (APC/C), a key cell-cycle regulator and tumor suppressor, had attenuated ligase activity in CSCs. Here, we assessed the mechanism of reduced activity, as well as the efficacy of pharmacologically targeting the APC/C in CSCs. We identified hyperphosphorylation of CDH1, but not pseudosubstrate inhibition by early mitotic inhibitor 1 (EMI1), as a major mechanism driving attenuated APC/C^{CDH1} activity in the G_1-phase of the cell cycle in CSCs. Small-molecule inhibition of the APC/C reduced viability of both CSCs and nonstem tumor cells (NSTCs), with the combination of proTAME and apcin having the biggest impact. Combinatorial drug treatment also led to the greatest mitotic arrest and chromosomal abnormalities.

Implications: Our findings demonstrate how the activity of the APC/C^{CDH1} tumor suppressor is reduced in CSCs and also validates small-molecule inhibition of the APC/C as a promising therapeutic target for the treatment of GBM.

Introduction

Glioblastoma (GBM) is the most lethal primary brain tumor with the common length of survival at only 12–15 months following diagnosis (1, 2). This poor prognosis is, in part, due to a highly malignant subpopulation of cells within these tumors called cancer stem–like cells (CSC). These cells are treatment resistant and are thought to drive tumor recurrence (3–6). Critical for tumor progression and treatment resistance is abnormal regulation of the cell cycle that is permissive for the background of inherent genomic instability common in cancer cells. This instability provides advantageous karyotypes favoring clonogenic outgrowth of resistant tumor cells (7, 8). GBM CSCs display heightened chromosomal instability (CIN), one form of genomic instability, with lagging chromosomes at anaphase and extensive nonclonal chromosome copy-number variations (9). When the inherent level of CIN was elevated in CSCs, their proliferation decreased and the stem-like phenotype of CSCs was impaired (9). Moreover, tumor formation was abolished in an orthotopic mouse model (9). These results demonstrate that CSCs generate genetic heterogeneity via CIN within tumors, but that CSC function is impaired if the rate of genetic change is elevated above a tolerable threshold.

One key component permissive to a tolerant proliferation state in the presence of CIN is the anaphase-promoting complex (also called the cyclosome or APC/C), an E3 ubiquitin ligase that targets cell-cycle proteins for proteasomal-mediated degradation (10). APC/C targets are differentially regulated throughout the cell cycle by two mutually exclusive activator proteins, CDC20 and CDH1. These proteins target the APC/C to specific sets of substrates at different times in the cell cycle, thus driving cell-cycle progression. Recently, APC/C activity has been shown to modulate the level of CIN between a viable or unviable state (10). Furthermore, APC/C^{CDH1} has been validated as a tumor suppressor with dysregulation of APC/C^{CDH1} contributing to tumor development (11, 12). Previously, we have demonstrated attenuated activity of APC/C^{CDH1} in GBM CSCs in the G_1-phase of the cell cycle, hence leading to elevated APC/C^{CDH1} substrates throughout the cell cycle, including CDC20 (13). CDC20 has been explored as a target in GBM and more specifically GBM CSCs with multiple groups using RNAi to CDC20 to demonstrate reduced CSC invasion, self-renewal, proliferation, and tumor initiation, collectively (14, 15).

In this study, we sought to determine the mechanism of dysregulation of APC/C^{CDH1} in GBM CSCs with the potential for the knowledge gained to provide fundamental mechanistic insight into cell-cycle regulation of CSCs and potentially reveal other therapeutic targets for GBM. We also took advantage of two

[1]Department of Radiation Oncology, James Cancer Hospital and Comprehensive Cancer Center, The Ohio State University, Columbus, Ohio. [2]Neuroscience Graduate Program, The Ohio State University, Columbus, Ohio. [3]Heritage College of Osteopathic Medicine, Ohio University, Athens, Ohio. [4]Department of Life Sciences, Presidency University, Kolkata, West Bengal, India.

Note: Supplementary data for this article are available at Molecular Cancer Research Online (http://mcr.aacrjournals.org/).

Corresponding Author: Monica Venere, The Ohio State University, 420 West 12th Ave, TMRF 514B, Columbus, OH 43210. Phone: 614-685-7842; Fax: 614-293-2770; E-mail: monica.venere@osumc.edu

Mol Cancer Res 2019;17:1519–30

doi: 10.1158/1541-7786.MCR-18-1361

Published OnlineFirst April 29, 2019; DOI: 10.1158/1541-7786.MCR-18-1361

recently developed APC/C inhibitors, namely proTAME and apcin, to explore the therapeutic potential of small-molecule inhibition of the APC/C in GBM.

Materials and Methods

Cell culture

Human GBM specimens were originally isolated from tumor resections in accordance with approved institutional review board protocols. Known tumor grade, available cytogenetic information (relevant to pathologic classification), and subtype classification (putative as based on xenograft passaged cells) for each specimen have been previously published and are summarized in Supplementary Table S1 (4, 13, 16). Tumor specimens were maintained through subcutaneous xenografts in the flanks of athymic nude mice (Crl:NU(NCr)-*Foxn1*^{nu}) or NOD *scid* gamma (NOD.*Cg-Prkdc*^{scid}*Il2rg*^{tm1Wjl}/SzJ) mice under approved institutional protocols and in accordance with the NIH Guide for the Care and Use of Laboratory Animals. Tumors were dissociated using a Papain Dissociation System (Worthington Biochemical). Enrichment of CD133-positive CSCs was achieved by magnetic-activated cell sorting for the CD133/1 (AC133) epitope as per the manufacturer's recommendations (MACS Miltenyi Biotec.). Matched NSTCs were subjected to two rounds of negative sorting for CD133/1 to remove any weakly CD133-positive cells. Cells were cultured at 37 °C at 5% CO_2. CSCs were cultured in Neurobasal Media (Gibco) with B-27 supplement (without vitamin A; Gibco), basic fibroblast growth factor (10 ng/mL; Gibco), EGF (10 ng/mL; Gibco), L-glutamine (2 mmol/L; Gibco), and sodium pyruvate (1 mmol/L; Gibco) and grown adherently on Geltrex LDEV-Free hESC-Qualified, Reduced Growth Factor Basement Membrane Matrix (Gibco). NSTCs were cultured in DMEM with L-glutamine and 4.5 g/L glucose (DMEM; Corning) with the addition of 10% FBS (Gibco). All CSCs and NSTCs were used within 10 passages post-sorting from the xenograft tumor. Primary normal human astrocytes were commercially obtained and grown in the recommended growth medium on Geltrex-Coated Plates (Lonza). For cell counting before each experiment, a single-cell suspension was achieved using TrypLE (Gibco). *Mycoplasma* testing was done quarterly (LookOut Mycoplasma PCR Detection Kit; Sigma-Aldrich) and cell line verification was done annually (microsatellite genotyping; OSUCCC Genomics Shared Resource).

Cell synchronization and extract preparation

CSCs and NSTCs were synchronized using media supplemented with 100 ng/mL nocodazole for 18 hours to arrest cells in mitosis followed by mitotic shake off and release in fresh medium for 4–6 hours to enrich for cells in early G_1 as reported previously (13). Validation of synchronization and G_1 enrichment for each experiment was achieved using propidium iodide to stain the DNA of fixed cells followed by analysis on the BD LSRII or the BD FACSCalibur Flow Cytometer (BD Biosciences). Whole-cell extracts were made using a 50 mmol/L Tris pH 8.0, 120 nmol/L NaCl, 0.5% NP-40 lysis solution supplemented with protease and phosphatase inhibitors (Roche).

Immunoprecipitation

Immunoprecipitations were carried out using Dynabeads Protein G (Invitrogen) except for endogenous CDH1 immunoprecipitation experiments for which Sera-Mag Magnetic SpeedBeads Protein A/G (GE Healthcare) were used. Briefly, 25 μL of beads were incubated with 1 μg of antibody for 30 minutes at room temperature followed by washes and then an overnight incubation at 4°C with 1–2.5 mg of CSC or NSTC whole-cell extract. Immunoprecipitated proteins were released from the beads by boiling in Laemmli 2× concentrate sample buffer (Sigma).

Immunoblotting

Samples were run on 7.5% SDS-PAGE gels or 4%–20% Mini-PROTEAN TGX Precast Gels (Bio-Rad Laboratories, Inc.) and transferred to Polyvinylidene diflouride membranes (Millipore Corp.). The membranes were blocked with 5% (w/v) BSA or 5% dry milk (as per the manufacturer's recommendation) in TBS-Tween-20 (TBST; 0.1%–0.2% vol/vol) and probed with primary antibodies overnight at 4°C. Secondary antibodies (LI-COR Biosciences) were incubated in TBST plus 0.01%–0.02% SDS and visualized with the LI-COR Odyssey near infrared imaging system. To circumvent the signal for the IgG heavy chain from masking our proteins of interest at that same molecular weight (~50 kDa) in experiments that utilized antibodies from the same species [i.e., immunoprecipitation with mouse anti-APC4 or anti-CDH1 followed by immunoblotting with mouse anti-CDH1 or anti-early mitotic inhibitor 1 (EMI1)], a Fab-fragmented antibody that reacts only with whole-molecule mouse IgG was used [Biotin-SP (long spacer) AffiniPure Fab Fragment anti-mouse IgG (H+L); Jackson ImmunoResearch Laboratories, Inc.] followed by secondary detection with IRDye 800CW Streptavidin (LI-COR Biosciences). To determine the relative stoichiometry of CDH1 or EMI1 bound to the APC/C holoenzyme between CSCs and NSTCs, resulting immunoprecipitates were run as described above and the band intensity for APC4 or CDC27 was obtained using the LI-COR Odyssey Image Studio software to represent the level of APC/C holoenzyme immunoprecipitated. The CDH1 or EMI1 band from that same immunoprecipitation was then measured and bound CDH1 or EMI1 was calculated to be (band intensity CDH1 or EMI1)/(band intensity APC4 or CDC27). This approach allows for the stoichiometry of bound CDH1 or EMI1 to be calculated independently within each cell type regardless of any potential differences in overall holoenzyme or subunit levels (17, 18–21).

Immunofluorescence

Cells were fixed in 100% methanol, permeabilized in PBS-Triton X-100 (0.2% vol/vol), and immunolabeled with anti-α-tubulin (Sigma-Aldrich) overnight at 4°C followed by secondary detection with Alexa Fluor 488 (Invitrogen) for 1 hour at room temperature. Nuclei were counterstained with Hoechst. Coverslips were then mounted onto slides using Fluoromount-G (SouthernBiotech). Images were taken using a Leica DM5500B upright epifluorescence microscope.

Silver staining

Following immunoprecipitation of the APC/C holoenzyme and sample separation by SDS-PAGE, the gel was incubated for 1 hour in 50% methanol and then incubated for 15 minutes in a mixture of freshly prepared staining solution (0.0472 mol/L $AgNO_3$, 10 N NaOH, and 14.8 mol/L ammonium hydroxide). The gel was then incubated in a freshly prepared solution of 1% citric acid and 38% formaldehyde to develop the signal. A 5% acetic acid solution was added to the gel to stop development. The gel was preserved in an 8.8% glycerol solution. All solutions were made with nuclease-free water.

Published OnlineFirst April 29, 2019; DOI: 10.1158/1541-7786.MCR-18-1361

Colony formation assay

Cells were seeded at 1,000 cells per well in 6-well plates. The next day, cells were treated twice for 24 hours with vehicle (DMSO), 12 μmol/L proTAME, 48 μmol/L apcin, or 12 μmol/L proTAME plus 48 μmol/L apcin. Twenty-four hours later, the wells were washed three times with 1× PBS and fresh media was added. After incubation for 14 days for CSCs and 21 days for NSTCs cells, the remaining colonies were washed twice with 1× PBS then stained with 0.5% crystal violet containing methanol for 15 minutes at room temperature. Image acquisition of remaining colonies was performed with the LI-COR Odyssey near infrared imaging system. Images were exported and quantified using Fiji software and surrogate analysis using total area as a derivative of colony number was performed using a custom macro to manually gate out background and mark colonies for each well.

Cell growth

Cells were seeded at 2,000 cells per well in 96-well plates. The next day, cells were treated with vehicle (DMSO), 12 μmol/L proTAME, 48 μmol/L apcin, or 12 μmol/L proTAME plus 48 μmol/L apcin. Cell confluence as a measure of cell growth over time was monitored every 4 hours for up to 4 days using the IncuCyte ZOOM Live-Cell Imaging System (Essen Biosciences). Alternatively, direct cell counts over time were obtained using the NucLight Rapid Red Reagent (Essen Biosciences).

Mitotic index

Following treatment with vehicle (DMSO), 12 μmol/L proTAME, 48 μmol/L apcin, or 12 μmol/L proTAME plus 48 μmol/L apcin for 6 or 24 hours, cells were harvested to a single-cell suspension and fixed overnight using ice-cold 70% ethanol. Cells were then stained with rabbit anti-phospho-Histone H3 (Ser10) XP Alexa Fluor 647 conjugate, clone D2C8 (1:100; Cell Signaling Technology) for 1 hour at room temperature, followed by 50 μg/mL propidium iodide incubation for 1 hour at room temperature. The mitotic index was quantified as the percentage of phospho-Histone H3 (Ser10)-positive cells as a total of all cells via analysis on the BD LSRII or the BD FACSCalibur Flow Cytometer (BD Biosciences).

Samples for LC/MS-MS analysis

The APC/C holoenzyme from G_1-synchronized CSCs and NSTCs was immunoprecipitated as described above with resulting immunoprecipitated proteins taken on beads for processing by the Proteomics Shared Resource at The Ohio State University Comprehensive Cancer Center for protein identification and quantification of protein abundance. For posttranslational modification analysis of CDH1, extracts were prepared for G_1-synchronized CSCs and NSTCs by resuspending cell pellets in extract buffer (20 mmol/L Tris-HCl, pH 7.2, 2 mmol/L DTT, 0.25 mmol/L EDTA, 5 mmol/L KCl, and 5 mmol/L $MgCl_2$) followed by two rounds of freeze-thaw and passage through a needle. Extracts were supplemented with ATP and an energy regenerating system. A total of 5 μg of recombinant GST-CDH1 fusion protein was then incubated with the extracts for 1 hour at 30°C and then captured on Glutathione beads. Samples were resolved on 4%–20% Mini-PROTEAN TGX Precast Gels (Bio-Rad Laboratories, Inc.) and visualized with GelCode Blue Stain Reagent as per the manufacturer's instructions (Thermo Fisher Scientific). The GST-CDH1 band was then cut from the gel and processed by the Lerner Research Institute Mass Spectrometry Laboratory for Protein Sequencing for proteomic analysis and quantification of posttranslational modifications on GST-CDH1.

Antibodies

Immunoprecipitation (all used at 1 μg per reaction): mouse anti-CDC27, clone AF3.1 (Sigma-Aldrich), mouse anti-APC4, clone CIV1.1 (Novus Biologicals), or mouse anti-CDH1, clone DH01 (Calbiochem/MilliporeSigma). Immunoblotting: mouse anti-CDC27, clone AF3.1 (1:1,000; Sigma-Aldrich), mouse anti-APC4, clone CIV1.1 (1:1,000; Novus Biologicals), mouse anti-CDH1, clone DH01 (1:1,000; Calbiochem/MilliporeSigma), mouse anti-EMI1, clone 3D2D6 (1:100; Zymed/LifeTech Sci), mouse anti-Phosphoserine, clone 4A4 (1:1,000; Sigma-Aldrich), rabbit anti-phospho-Histone H3 (Ser10), clone 63-1C-8 (1:1,000; Millipore), mouse anti-β-actin (1:20,000; Sigma-Aldrich), mouse anti-α-tubulin (1:10,000; Sigma-Aldrich), Biotin-SP (long spacer) AffiniPure Fab Fragment anti-mouse IgG (H+L) (1:5,000; Jackson ImmunoResearch Laboratories, Inc.), IRDye 800CW Goat anti-Rabbit IgG (H + L), IRDye 800CW Goat anti-Mouse IgG (H + L), and IRDye 800CW Streptavidin (1:15,000; LI-COR Biosciences). Immunofluorescence: mouse anti-α-tubulin (1:1,000; Sigma-Aldrich), and Alexa Fluor 488 (1:500; Invitrogen). Flow cytometry: rabbit anti-phospho-Histone H3 (Ser10) XP Alexa Fluor 647 conjugate and clone D2C8 (1:100; Cell Signaling Technology).

Small-molecule inhibitors

Apcin was purchased from R&D Systems and was resuspended in DMSO to a 50 mmol/L stock solution. proTAME was purchased from Boston Biochem, Inc. and was received as a 20 mmol/L stock solution in DMSO. Both drugs were diluted to working concentrations according to the manufacturer's instructions.

Statistical analyses

Statistical significance was calculated with GraphPad prism software using a one- or two-way ANOVA with Bonferroni or Dunnett posttest or a Student *t* test where appropriate (GraphPad Software, Inc.).

Results

The fraction of active APC/C is reduced in G_1 in GBM CSCs

It is well established that KIF11 is a substrate of APC/C^{CDH1} and is degraded as cells transition from mitosis to G_1 when the function of KIF11 as a key mediator of mitotic progression is no longer required (22, 23). We previously demonstrated that the ligase activity of APC/C^{CDH1} is attenuated in the G_1-phase of the cell cycle in GBM CSCs compared with matched nonstem tumor cells (NSTC) leading to elevated levels of KIF11 and other APC/C^{CDH1} substrates throughout the cell cycle (13). To begin to understand how the activity of APC/C^{CDH1} is attenuated in CSCs, we evaluated the stoichiometry of the APC/C holoenzyme, which is composed of over a dozen subunits, between CSCs and NSTCs sorted from patient-derived, xenograft-passaged (PDX) specimens. Cells were arrested in early mitosis via a nocodazole block then released and harvested approximately 5 hours later when cells were enriched in early G_1 as confirmed by flow cytometry (Supplementary Figs. S1 and S2). The APC/C holoenzyme was immunoprecipitated and levels of the subunits determined by silver stain (Fig. 1A) or by mass spectrometry (Fig. 1B). In both assays, the APC/C components identified were higher in CSCs

Published OnlineFirst April 29, 2019; DOI: 10.1158/1541-7786.MCR-18-1361

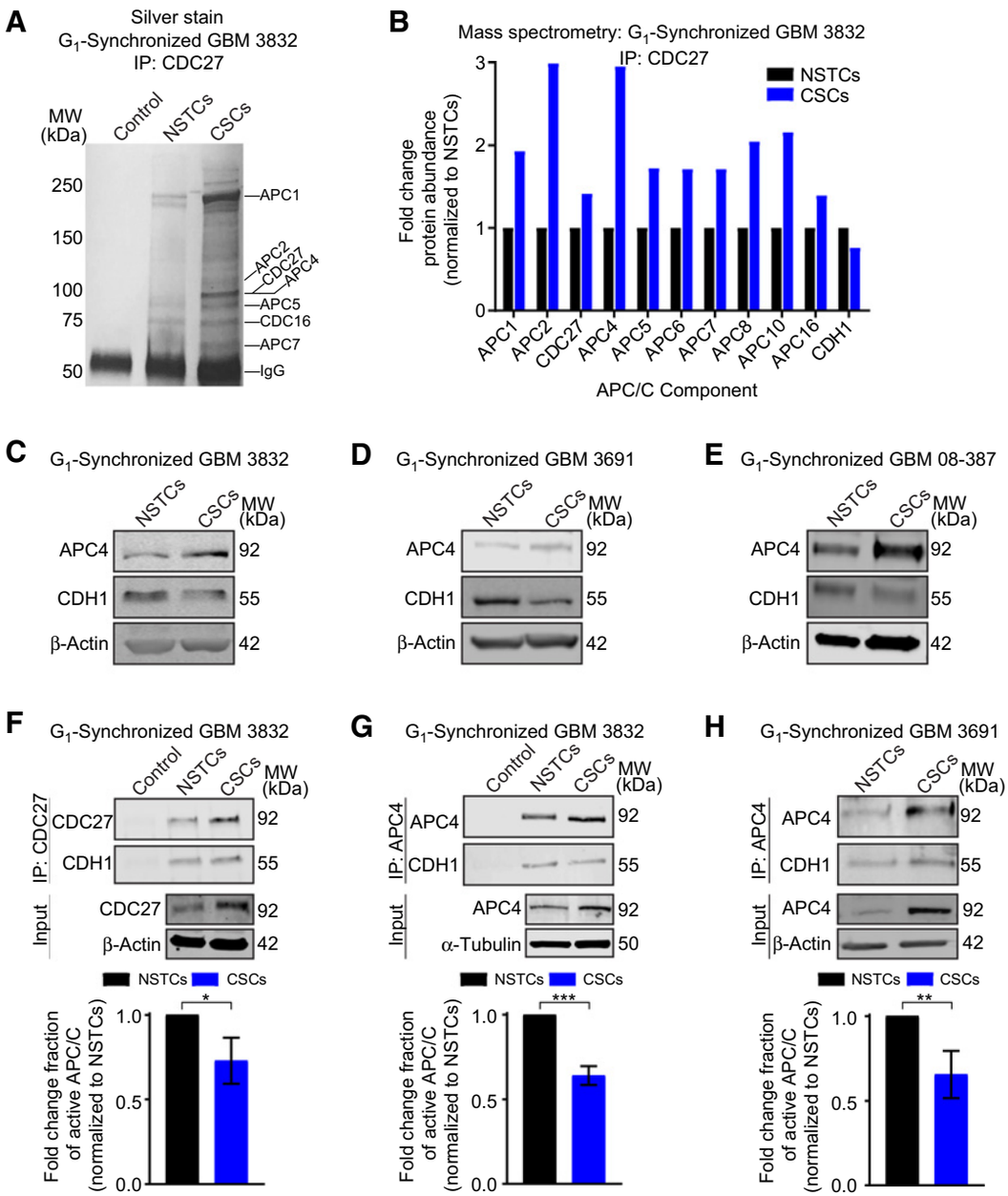

Figure 1.

The APC/C holoenzyme is upregulated in CSCs but the fraction of active APC/C is reduced in G_1. **A,** The APC/C holoenzyme was immunoprecipitated (IP) using anti-CDC27 from G_1-synchronized NSTCs and CSCs from GBM 3832 with resulting levels of the indicated APC/C subunits identified by silver staining. Control lane, anti-CDC27 antibody and beads only. Antibody heavy chain is indicated (IgG). **B,** The APC/C holoenzyme was immunoprecipitated using anti-CDC27 from G_1-synchronized NSTCs and CSCs from GBM 3832 with resulting immunoprecipitates analyzed by LC/MS-MS. Protein abundance for the indicated APC/C holoenzyme subunits and CDH1 were quantified and resulting fold change graphed (normalized to the NSTCs). Whole-cell lysates from G_1-synchronized NSTCs and CSCs from GBM 3832 (**C**), 3691 (**D**), and 08-387 (**E**) were probed for APC4 and CDH1. β-Actin served as a loading control. The APC/C holoenzyme was immunoprecipitated from G_1-synchronized NSTCs and CSCs from GBM 3832 using anti-CDC27 (**F**) or anti-APC4 (**G**) and from 3691 using anti-APC4 (**H**). Resulting immunoprecipitates were probed for CDC27 or APC4 and CDH1 (top two panels). Control lane, anti-CDC27 or anti-APC4 antibody and beads only. Bound CDH1 relative to CDC27 or APC4 as an indication of active APC/C was quantified and resulting fold change graphed (normalized to NSTCs). $n = 3$ biological replicates; error bars, SD; *, $P < 0.05$; **, $P < 0.01$; ***, $P < 0.001$. Bottom two panels represent inputs for the CDC27 or APC4 immunoprecipitation. β-Actin or α-tubulin served as loading controls. For all immunoblots, the molecular weight (MW) of resulting bands is given in kilodaltons (kDa).

Published OnlineFirst April 29, 2019; DOI: 10.1158/1541-7786.MCR-18-1361

over NSTCs. However, proteomic analysis indicated that the APC/C-associated CDH1 levels were decreased in CSCs. We confirmed elevated levels of the APC/C subunit APC4 and decreased levels of CDH1 in CSCs from three independent PDX specimens (Fig. 1C–E). These data indicate that although apo-APC/C (i.e., ligase minus the activator protein) is overexpressed in CSCs compared with NSTCs, total CDH1 levels are somewhat reduced.

We were next interested in evaluating the level of interaction between the APC/C and CDH1, as CDH1 provides substrate recognition and consequential ubiquitination of target proteins by APC/C^{CDH1}. CSCs and NSTCs were enriched in early G_1 following a nocodazole block and release, and the APC/C was isolated via immunoprecipitation with antibodies to CDC27 or APC4 from two different patient specimens. Resulting immunoprecipitates were probed for the APC/C component used for immunoprecipitation as well as CDH1. The level of APC/C bound CDH1 was quantified and demonstrated approximately half of the binding to the holoenzyme as compared with NSTCs in all experiments (Fig. 1F–H). These data indicate that the interaction between the APC/C and CDH1 is attenuated in GBM CSCs, which results in an overall attenuated activity of APC/C^{CDH1} in G_1.

CDH1 is hyperphosphorylated in GBM CSCs

For efficient cell-cycle progression to occur, APC/C^{CDH1} activity is greatly reduced as cells transition from G_1 to S-phase (24, 25). One major mechanism used to achieve this reduced activity is hyperphosphorylation of CDH1 by cyclin-dependent kinases (CDK) in late G_1, which prevents the interaction of CDH1 with the APC/C (24–28). To explore the hypothesis that reduced CDH1 binding to the APC/C in CSCs is due to aberrant hyperphosphorylation in early G_1, we immunoprecipitated CDH1 from CSCs and NSTCs from three different PDX specimens and immunoblotted with a pan phospho-serine antibody. In all three PDX specimens, CDH1 was hyperphosphorylated in CSCs compared with NSTCs (Fig. 2A–C). We also evaluated the level of kinase activity toward CDH1 in early G_1 and preferential sites of phosphorylation using an *in vitro* extract assay and mass spectrometry. Cell lysates were harvested from G_1-synchronized CSCs and NSTCs and then recombinant GST-CDH1 was incubated in the lysates and later captured on glutathione beads. The isolated GST-CDH1 was then analyzed by mass spectrometry to identify the overall level of phosphorylation on CDH1, as well as the sites targeted for phosphorylation between CSCs and NSTCs (Fig. 2D). Results indicated that CDH1 was hyperphosphorylated in CSCs in early G_1 as compared with NSTCs with the majority of the sites identified previously reported as CDK consensus sites on CDH1 (28). Two of the upregulated sites, S40 and S151, are known to regulate binding of CDH1 to the APC/C (29). These results support hyperphosphorylation of CDH1 in CSCs as a contributing factor to the reduced interaction between CDH1 and the APC/C in early G_1 and hence overall attenuated ligase activity.

EMI1 protein levels are higher in GBM CSCs in G_1 but there is no increased binding to the APC/C

APC/C^{CDH1} activity in late G_1 is also inhibited by EMI1 via its ability to directly bind CDH1 and prevent recruitment of APC/C^{CDH1} substrates, as well as its association with core APC/C subunits to suppress ligase activity (30). To evaluate whether pseudosubstrate inhibition by Emi1 could also be contributing to attenuated APC/C^{CDH1} activity in early G_1 in CSCs, we first evaluated overall EMI1 levels between CSCs and NSTCs. In all three PDX specimens evaluated, EMI1 levels were higher in CSCs (Fig. 3A–C). To check the level of association of EMI1 to the APC/C, we immunoprecipitated the holoenzyme from G_1-enriched CSCs and NSTCs and immunoblotted for EMI1. Despite overall higher EMI1 levels in CSCs, we did not identify any differences in the binding pattern of EMI1 to the APC/C between NSTCs and CSCs (Fig. 3D and E). These result support hyperphosphorylation of CDH1 as the main mechanism of attenuated APC/C^{CDH1} activity in early G_1 over pseudosubstrate inhibition by EMI1.

Combination treatment with the APC/C inhibitors proTAME and apcin has the greatest impact on CSC viability

We previously reported that the altered regulation of APC/C^{CDH1} led to increased levels of substrates, including CDC20 (13). This finding, along with previous reports highlighting CDC20 as a promising target in GBM and GBM CSCs, prompted us to explore the efficacy of small-molecule inhibition of the APC/C in GBM CSCs and NSTCs (14, 15). Two APC/C inhibitors have been developed, namely proTAME and apcin (31, 32, 17). Both apcin, which disrupts the interaction of CDC20 with APC/C substrates, and proTAME, which disrupts the interaction between APC/C and CDC20 or CDH1, previously demonstrated an impact on mitotic progression (17). These drugs also led to increased cell death when tested *in vitro* on multiple myeloma cells and osteosarcoma cells (33, 34). We first performed a colony formation assay on CSCs and NSTCs from two independent PDX specimens that were treated with vehicle (DMSO), 12 μmol/L proTAME, 48 μmol/L apcin, or the combination of proTAME and apcin, with the concentrations used on the basis of previous reports and calculated dose–response curves for CSCs and NSTCs, which fell within or just outside of the range of the concentrations used in previous reports (Supplementary Fig. S3; refs. 26, 28). Clonogenic survival was significantly reduced for both CSCs and NSTCs exposed to proTAME and the combination, with no significant impact seen with apcin alone (Fig. 4A–D). We also monitored cell growth over a 4-day time course for CSCs and NSTCs that were given a single exposure to vehicle, 12 μmol/L proTAME, 48 μmol/L apcin, or the combination and again saw the greatest impact on cell growth when the drugs were used in combination (Fig. 4E and F; Supplementary Figs. S4 and S5). proTAME alone, but not apcin alone, was able to significantly compromise cell growth in CSCs and NSTCs. In testing of drug treatment on primary normal human astrocytes, the combination treatment did have an impact on cell growth (Supplementary Fig. S6). Together these data underscore the utility of targeting the APC/C to compromise growth of both CSCs and NSTCs, and hence positions this targeted approach as a promising therapeutic modality for GBM, although future preclinical studies will need to closely evaluate the impact of treatment on nonneoplastic brain cells.

Combination treatment leads to mitotic arrest and gross chromosomal abnormalities in GBM cells

The main impact of APC/C inhibition on cell-cycle progression by proTAME and apcin was reported to be prolonged arrest in mitosis at metaphase due to lack of APC/C^{CDC20} to degrade substrates needed for progression to anaphase (32, 17). To confirm the mechanism of action of proTAME and apcin in CSCs and NSTCs we assessed the mitotic index using flow cytometry for phospho-Histone3 serine10 (pH3S10) at 6 and 24 hours following treatment with vehicle, 12 μmol/L proTAME, 48 μmol/L

Published OnlineFirst April 29, 2019; DOI: 10.1158/1541-7786.MCR-18-1361

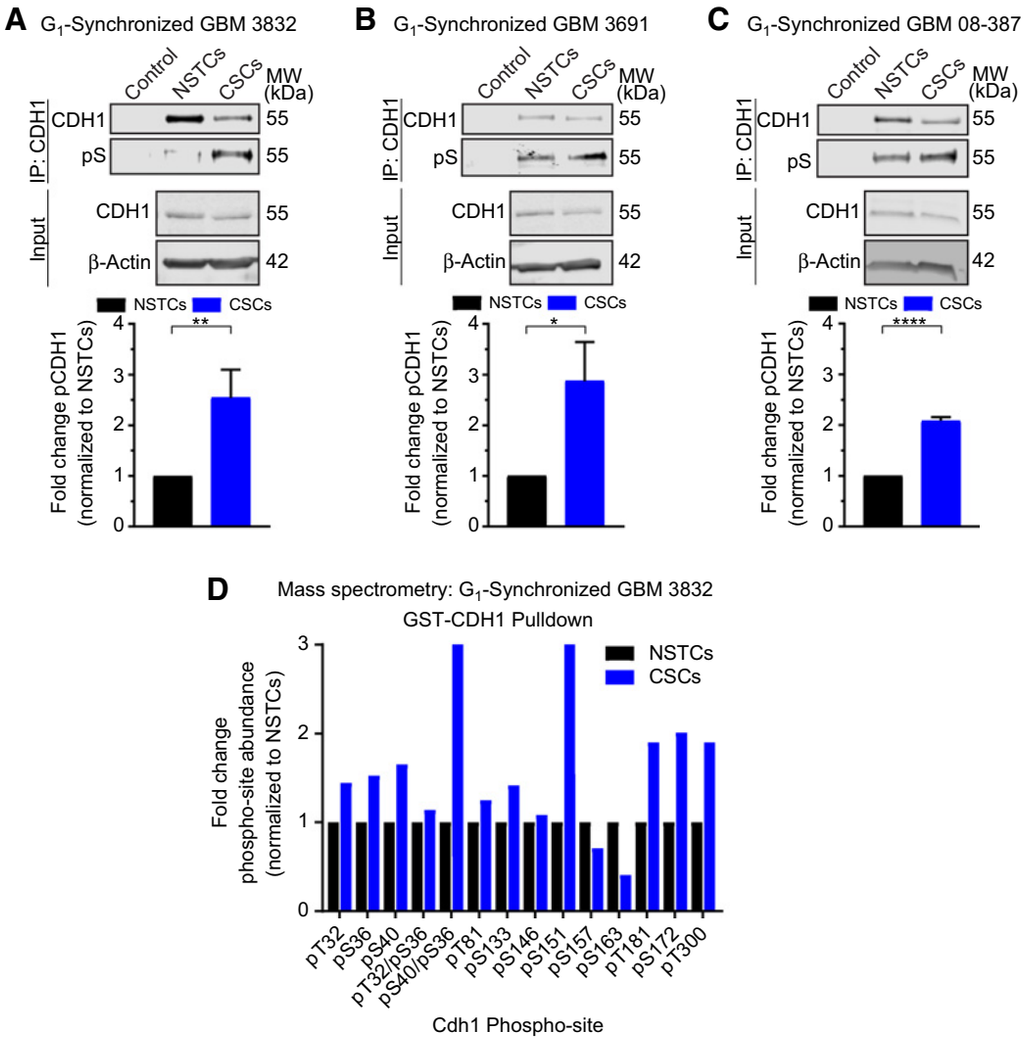

Figure 2.

CDH1 phosphorylation is elevated in CSCs. CDH1 was immunoprecipitated (IP) from G_1-synchronized NSTCs and CSCs from GBM 3832 (**A**), 3691 (**B**), and 08-387 (**C**). Resulting immunoprecipitates were probed for CDH1 and phospho-Serine (pS; top two panels). Control lane, anti-CDH1 antibody and beads only. pS relative to total CDH1 was quantified and resulting fold change graphed (normalized to NSTCs). $n = 3$ (3691 and 08-387) or $n = 4$ (3832) biological replicates; error bars, SD; *, $P < 0.05$; **, $P < 0.01$; ****, $P < 0.0001$. Bottom two panels represent inputs for the CDH1 immunoprecipitation. β-Actin served as a loading control. The molecular weight (MW) of resulting bands is given in kilodaltons (kDa). **D,** Recombinant GST-CDH1 was incubated with whole-cell lysate from G_1-synchronized NSTCs and CSCs from GBM 3832 then isolated using glutathione beads. GST-CDH1 was analyzed by LC/MS-MS for phosphorylation events. Resulting fold change in phospho-site abundance relative to total GST-CDH1 for the indicated phospho-epitopes identified was graphed (normalized to NSTCs).

apcin, or the combination. The greatest increase in the mitotic fraction was seen for cells treated with the combination at 6 hours for both cell types and also at 24 hours for CSCs (Fig. 5A). proTAME alone yielded a significant increase in mitotic cells for both CSCs and NSTCs at the 6 hour timepoint (Fig. 5A). The increase in mitotic arrest was confirmed by immunoblotting for pH3S10 (Fig. 5B and C). Using immunofluorescence, we also confirmed that cells treated with the combination had the greatest percent of mitotic cells that were arrested at metaphase in CSCs and NSTCs, specifically at the 6 hour timepoint and most significantly with the combination treatment for both cell types (Fig. 5D and E). During the scoring of cells for metaphase arrest, we noted that a large percentage of the CSCs had abnormal mitotic structures, such as multipolar spindles or misaligned chromosomes. When scored, these chromosomal abnormalities were observable and significantly increased with proTAME alone or the combination at 6 and 24 hours for CSCs and at the 6 hour timepoint only for NSTCs (Fig. 5F and G). Additional quantification for mitotic abnormalities in CSCs at, 48, 72, and 96 hours following single-drug exposure indicated a significant and sustained impact on mitotic fidelity with the combination drug treatment (Supplementary Fig. S7). These data support impaired mitotic progression and the induction of chromosomal abnormalities as the mechanism behind cell death caused by APC/C inhibition in GBM cells.

Published OnlineFirst April 29, 2019; DOI: 10.1158/1541-7786.MCR-18-1361

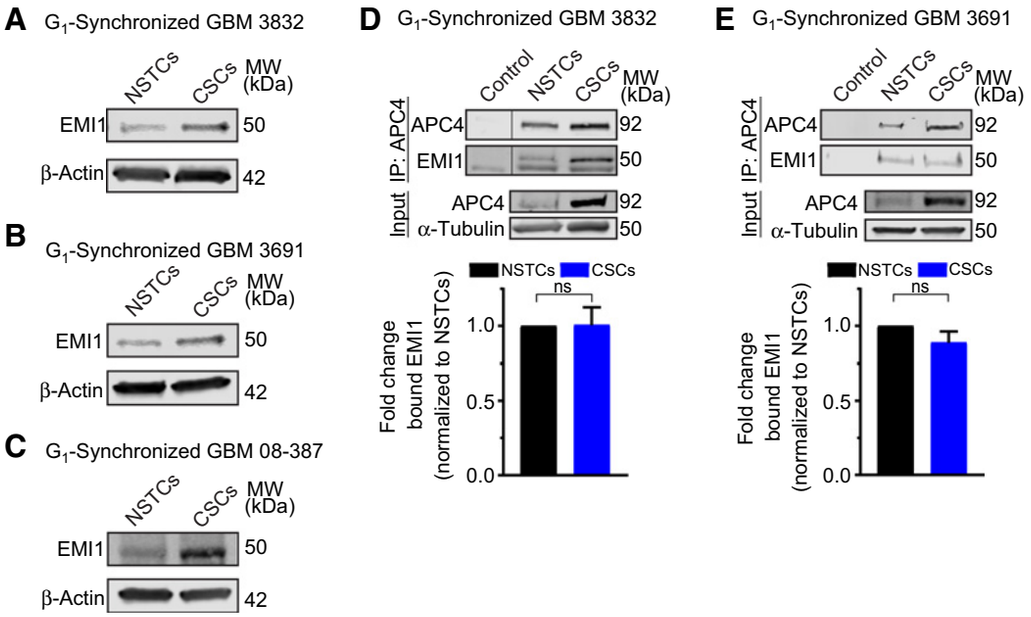

Figure 3.

EMI1 is overexpressed in GBM CSCs but does not have higher occupancy on the APC/C. Whole-cell lysates from G_1-synchronized NSTCs and CSCs from GBM 3832 (**A**), 3691 (**B**), and 08-387 (**C**) were probed for EMI1. β-Actin served as a loading control. The APC/C holoenzyme was immunoprecipitated (IP) from G_1-synchronized NSTCs and CSCs from GBM 3832 (**D**) or 3691 (**E**) using anti-APC4. Resulting immunoprecipitates were probed for APC4 and EMI1 (top two panels). Control lane, anti-APC4 antibody and beads only. The line in **D** indicates that two nonrelevant lanes were removed from the image between the control lane and the 3832 immunoprecipitation lanes. Bound EMI1 relative to APC4 was quantified and resulting fold change graphed (normalized to NSTCs). $n = 3$ biological replicates; error bars, SD; ns, no significance. Bottom two panels represent input for EMI1 immunoprecipitation. α-Tubulin served as a loading control. For all immunoblots, the molecular weight (MW) of resulting bands is given in kilodaltons (kDa).

Discussion

The lack of curative therapies for GBM supports continued exploration of the inherent biology of these tumors, as well as the development of novel therapeutic interventions. This is of particular importance in the context of CSCs for which resistance to current treatment paradigms has been extensively reported (3–6). We previously demonstrated attenuated activity of APC/C^{CDH1} in GBM CSCs as compared with NSTCs (13). This attenuated activity resulted in the levels of APC/C^{CDH1} mitotic substrates to remain elevated in G_1 (13). We have now expanded on this finding to identify hyperphosphorylation of CDH1 in early G_1 as a contributing mechanism to the overall reduced APC/C^{CDH1} ligase activity. Furthermore, we have validated small-molecule inhibition of the APC/C as a viable therapeutic approach to target CSC as well as NSTC viability.

It is well established that in normal cells, phosphorylation of CDH1 at the G_1–S-transition is driven by Cyclin–CDK complexes and is required to dissociate CDH1 from the APC/C and hence reduce ligase activity to allow accumulation of proteins needed for S-phase progression (24, 27, 35–38). APC/C^{CDH1} activity can also be reduced by CDH1 phosphorylation events that lead to decreased CDH1 stability or drive localization changes of CDH1 between the nucleus and cytoplasm (36, 39–41). We observed an increase in CDH1 phosphorylation and a concordant decreased binding of CDH1 to the APC/C, but of note, all of our studies were focused on APC/C^{CDH1} in early G_1, just after cells have transitioned from mitosis, and not at the G_1–S-transition where phosphorylation on CDH1 normally would occur. Furthermore, proteomics analysis identified an increase in numerous phosphoepitopes on CDH1 in GBM CSCs including several residues in the N-terminus known to disrupt the CDH1–APC/C interaction (29, 42, 43). Notably, phosphorylation of S133 and S172, two previously uncharacterized events, also perturbs the binding of CDH1 to APC/C (D. Pal and M.K. Summers, manuscript submitted). Hence, our findings support a model whereby aberrant kinase activity in GBM CSCs contributes to altered APC/C^{CDH1} activity in these cells. In support of this, two recent reports have highlighted elevated CyclinD-CDK4/6 activity in human cancer cells as being responsible for inactivating APC/C^{CDH1} via hyperphosphorylating CDH1 (42, 43). The CyclinD–CDK4/6–Rb axis is known to be disrupted in nearly 80% of GBMs via deletion of the INK4 locus or, less commonly, amplification of CDK4, CDK6, or Cyclin genes (44–46). Resolution of differences in CDK4/6 activity between CSCs and NSTCs is currently unknown, but it is known that CDK5 levels and activity are elevated in GBM CSCs (47). This is relevant in the context of CDH1 activity, as it has recently been shown that in postmitotic neurons CDK5 can phosphorylate CDH1 and inactivate APC/C^{CDH1} (48). It is therefore possible that elevated CDK5 in CSCs may contribute to CDH1 hyperphosphorylation. Further work is needed to elucidate the kinase(s) responsible for increased phosphorylation on CDH1 in CSCs. Furthermore, modulating the activity of these kinases to reduce phosphorylation on CDH1 and/or overexpressing CDH1 or phosphorylation-null mutants, and hence rescuing APC/C^{CDH1} activity in G_1, will be key future studies to elucidate how restoring

Published OnlineFirst April 29, 2019; DOI: 10.1158/1541-7786.MCR-18-1361

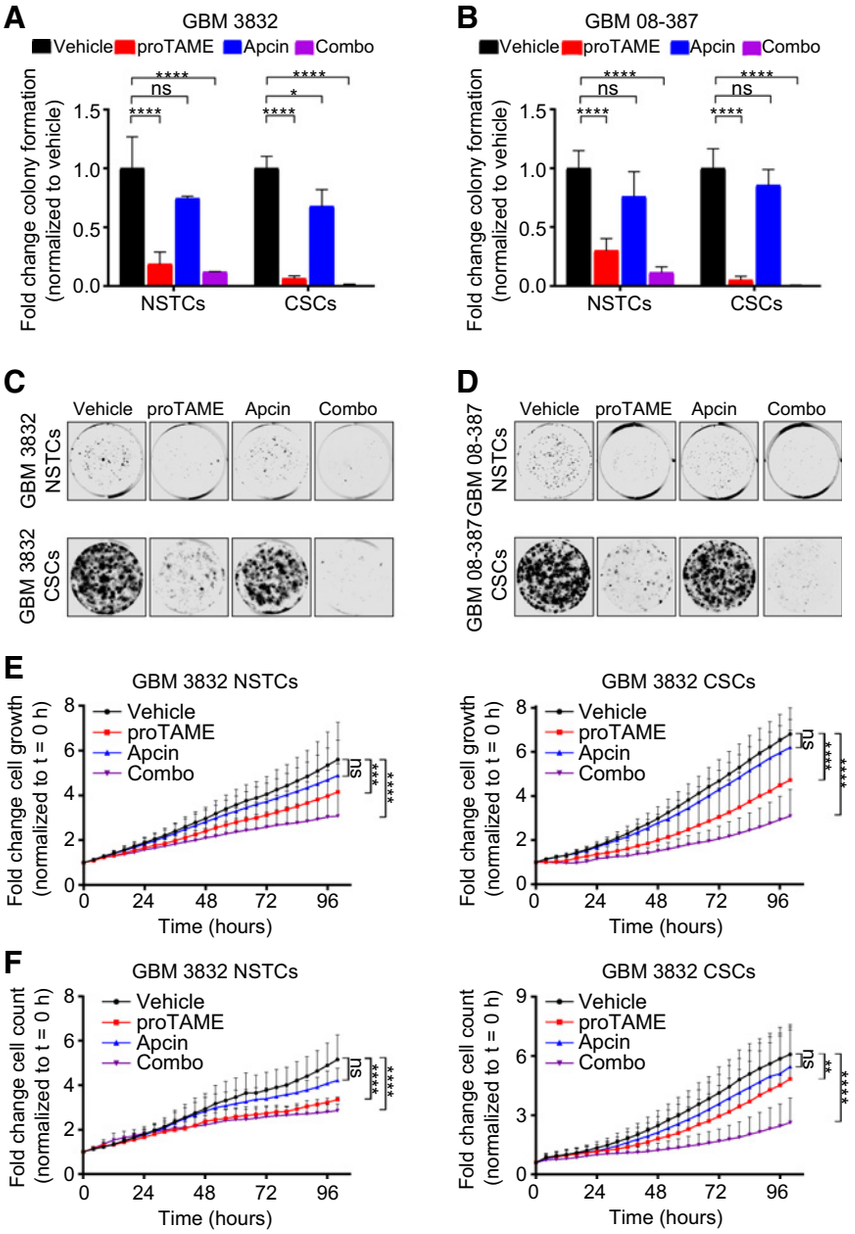

Figure 4.

GBM NSTCs and CSCs have decreased clonogenic survival and viability following APC/C inhibition. **A–D,** Clonogenic survival for NSTCs and CSCs from GBM 3832 and 08-387 was evaluated by colony formation following treatment with vehicle (DMSO), 12 μmol/L proTAME, 48 μmol/L apcin, or 12 μmol/L proTAME + 48 μmol/L apcin (combo). Fold change in colony formation for vehicle (black bars), proTAME (red bars), apcin (blue bars), and combo (purple bars) were graphed for 3832 (**A**) and 08-387 (**B**) NSTCs and CSCs (normalized to vehicle). $n = 3$ biological replicates (with three technical replicates per biological replicate); error bars, SD; *, $P < 0.05$; ****, $P < 0.0001$. Representative images of colony formation following each treatment are shown for 3832 (**C**) and 08-387 (**D**) NSTCs and CSCs. Cell growth was tracked for 100 hours measuring confluence (**E**) or direct cell count via NucLight Rapid Red Reagent (**F**) using the IncuCyte live-cell imaging system for NSTCs and CSCs from GBM 3832 following treatment with vehicle (DMSO), 12 μmol/L proTAME, 48 μmol/L apcin, or 12 μmol/L proTAME + 48 μmol/L apcin (combo). Fold change in cell growth via confluence or direct cell count for vehicle (black line), proTAME (red line), apcin (blue line), and combo (purple line) were graphed for 3832 NSTCs and CSCs. $n = 6$ biological replicates for **E** and $n = 3$ biological replicates for **F** (with three technical replicates per biological replicate; error bars, SD; ns, no significance; *, $P < 0.05$; **, $P < 0.01$; ***, $P < 0.001$; ****, $P < 0.0001$).

APC/C^{CDH1} activity in CSCs may impact the accumulation of mitotic abnormalities and overall genomic instability.

In addition, other factors may be contributing to attenuated activity of APC/C^{CDH1} toward its substrates in GBM CSCs such as reduced CDC14 phosphatase activity, increased activity of deubiquitinating enzymes, or even altered autoregulation of APC/C E2s (49). We did, however, validate that pseudosubstrate inhibition by EMI1 was not a major contributor to APC/C inhibition in early G_1, despite elevated EMI1 levels in CSCs. These findings are consistent with the fact that EMI1 is an APC/C^{CDH1} substrate in early G_1 and switches to an inhibitor in late G_1 as cells commit to the cell cycle (29, 50, 51). Thus, the elevated levels of EMI1 in CSCs likely reflects the diminished APC/C^{CDH1} activity and may function later to enhance cell-cycle progression. Alternatively, our EMI1 results could signify the importance of CDH1 phosphorylation in regulating a previously identified EMI1-independent pool of APC/C (29, 52, 53). Taken together, our work highlights that the level of CDH1 phosphorylation is a key contributor to attenuated APC/C^{CDH1} activity in G_1 and is, at least in part, causative for elevated levels of APC/C^{CDH1} substrates in CSCs.

Our study also highlights the utility of small-molecule inhibition of APC/C$^{CDH1/CDC20}$ as a therapeutic strategy to target CSCs in GBM. Elevated *CDC20* expression has previously been correlated with high grade glioma, as well as poor patient prognosis by a number of groups (54–57). We and others have shown that CDC20 is higher in CSCs over NSTCs and, more recently, RNAi has validated CDC20 as a critical modulator of the CSC phenotype (13–15). In our study, we tested the impact of two small-molecule inhibitors to the APC/C, proTAME and apcin, on CSC and NSTC viability. Apcin inhibits APC/C^{CDC20} by directly

Published OnlineFirst April 29, 2019; DOI: 10.1158/1541-7786.MCR-18-1361

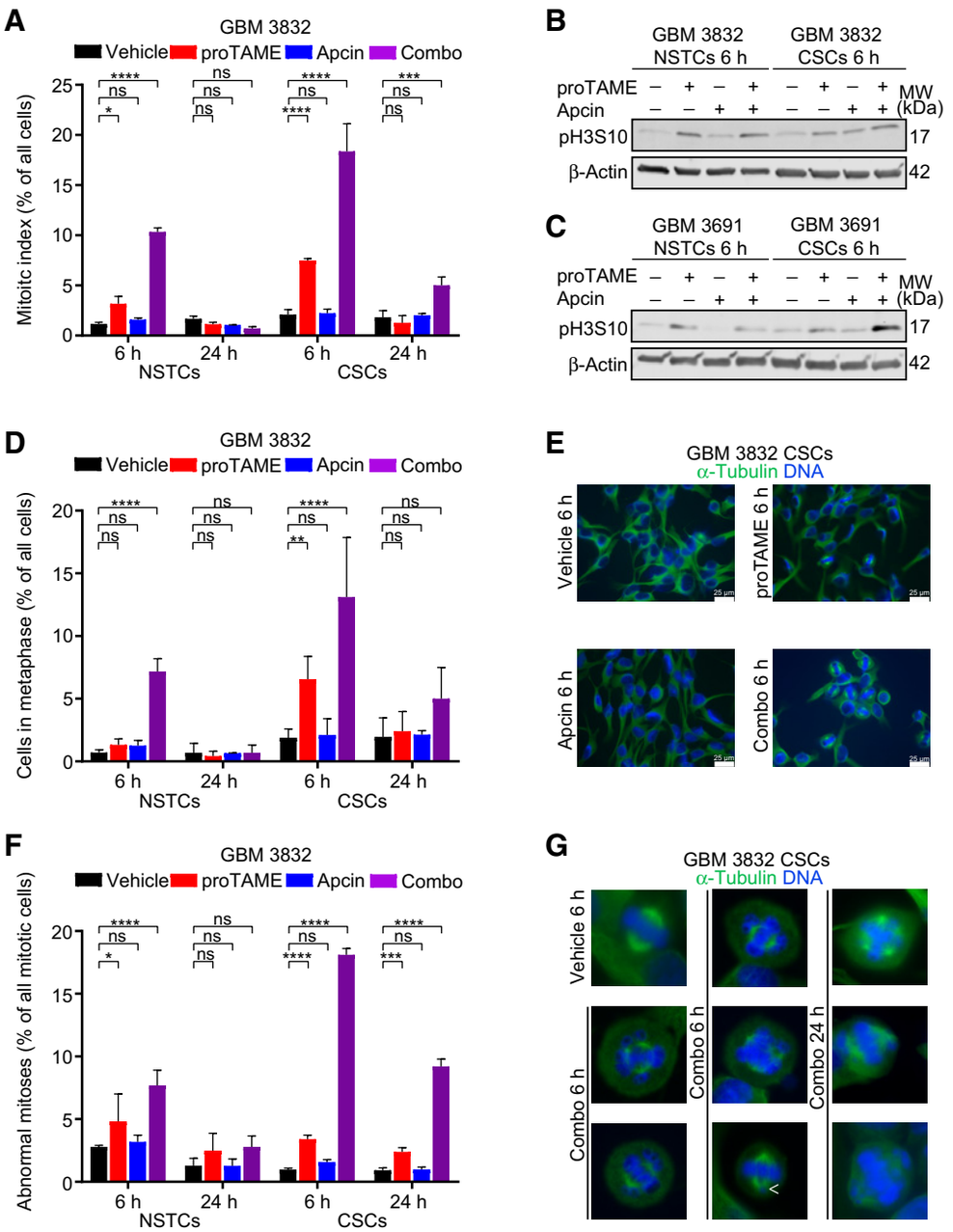

Figure 5.

APC/C inhibition leads to an increased number of cells in mitosis and mitotic abnormalities. **A,** The percent of cells in mitosis was quantified by flow cytometry for NSTCs and CSCs from GBM 3832 following 6 or 24 hours of treatment with vehicle (DMSO, black bar), 12 μmol/L proTAME (red bar), 48 μmol/L apcin (blue bar), or 12 μmol/L proTAME + 48 μmol/L apcin (combo, purple bar). $n = 3$ biological replicates; error bars, SD; ns, no significance; *, $P < 0.05$; ***, $P < 0.001$; ****, $P < 0.0001$. Whole-cell lysates from NSTCs and CSCs from GBM 3832 (**B**) and 3691 (**C**) treated for 6 hours with vehicle (DMSO), 12 μmol/L proTAME, 48 μmol/L apcin, or 12 μmol/L proTAME + 48 μmol/L apcin were probed for pH3S10. β-Actin served as a loading control. The molecular weight (MW) of resulting bands is given in kilodaltons (kDa). **D,** The percent of cells in metaphase was quantified for NSTCs and CSCs from GBM 3832 following 6 or 24 hours of treatment with vehicle (DMSO, black bar), 12 μmol/L proTAME (red bar), 48 μmol/L apcin (blue bar), or 12 μmol/L proTAME + 48 μmol/L apcin (combo, purple bar). Cells were processed for immunofluorescence to α-tubulin with DNA counterstained with Hoescht to identify metaphase cells. $n = 3$ biological replicates, between 100 and 200 cells were counted per replicate; error bars, SD; ns, no significance; **, $P < 0.01$; ****, $P < 0.0001$. **E,** Representative images of cells from each treatment group for CSCs. **F,** The percent of mitotic cells with abnormal chromosomal structures was quantified for NSTCs and CSCs from GBM 3832 following 6 or 24 hours of treatment with vehicle (DMSO, black bar), 12 μmol/L proTAME (red bar), 48 μmol/L apcin (blue bar), or 12 μmol/L proTAME + 48 μmol/L apcin (combo, purple bar). Cells were processed for immunofluorescence to α-tubulin with DNA counterstained with Hoescht to identify mitotic cells. $n = 3$ biological replicates, between 100 and 200 cells were counted per replicate; error bars, SD; ns, no significance; *, $P < 0.05$; ***, $P < 0.001$; ****, $P < 0.0001$. **G,** Representative images of a vehicle-treated cell at 6 hours and combo-treated cells at 6 and 24 hours for CSCs. White arrow head indicates a single unaligned chromosome.

Published OnlineFirst April 29, 2019; DOI: 10.1158/1541-7786.MCR-18-1361

binding CDC20 and preventing CDC20 substrate recognition (17). proTAME, which is processed to the active form of TAME by intracellular esterases, inhibits both APC/C^{CDH1} and APC/C^{CDC20} by disrupting the interaction of the coactivators with the APC/C (32). Elegant work exploring the precise mechanism of action for apcin demonstrated that APC/C substrates can outcompete apcin binding to CDC20 and/or the substrates may be recruited to the APC/C through other mechanism and hence allow for mitotic progression in the presence of apcin instead of mitotic arrest and subsequent death (17). It was also shown that the addition of proTAME enhanced the impact of apcin as proTAME inhibits CDH1/CDC20 via a distinct mechanism from apcin (17). Therefore, these drugs can elicit a mitotic arrest independently, but a greater impact on both mitotic arrest and cell death is seen when the drugs are used in combination and APC/C^{CDC20} is more efficiently inhibited (17, 33). Our studies are the first to demonstrate an impact on GBM cell viability using these inhibitors and support these previous findings whereby we observed the greatest impact on both CSC and NSTC mitotic progression and cell growth when apcin and proTAME were used in combination. Our studies also indicated that the drug combination had an impact on normal human astrocytes *in vitro*. As astrocytes are not continually proliferating *in vivo* as they are in the mitogenic environment of tissue culture, we expect to see less of an impact on nonneoplastic glial/neuronal cells when APC/C inhibitors are preclinically tested. However, side effects in consistently cycling tissues that are commonly impacted with chemotherapeutics designed to target proliferation would need to be closely evaluated.

We also observed a high percentage of CSCs that displayed mitotic abnormalities as early as 6 hours after combination drug treatment. These results indicate that GBM cells, and in particular GBM CSCs, are highly sensitive to perturbation of mitotic progression. More in-depth studies will be required, but these data support APC/C inhibition as a means to push CIN in GBM CSCs to an unviable state. The current APC/C inhibitors have not demonstrated bioavailability to our knowledge but, nonetheless, our work provides rationale for the further development and testing of APC/C inhibitors for GBM. Alternatively, delivery methods such as nanoparticles, liposomes, or convection-enhanced delivery may circumvent the issues with systemic delivery and warrant preclinical exploration. In summary, we have identified hyperphosphorylation of CDH1 as a mechanism driving attenuated activity of the tumor suppressor APC/C^{CDH1} in GBM CSCs. This results in elevated levels of APC/C^{CDH1} substrates, including CDC20. We also demonstrate that small-molecule inhibition of APC/$C^{CDH1/CDC20}$ can increase mitotic abnormalities and reduce CSC viability.

Disclosure of Potential Conflicts of Interest

No potential conflicts of interest were disclosed.

Disclaimer

The content is solely the responsibility of the authors and does not necessarily represent the official views of the NIH.

Authors' Contributions

Conception and design: K. De, M.K. Summers, M. Venere
Development of methodology: K. De, D. Pal, S. Majumder, M.K. Summers, M. Venere
Acquisition of data (provided animals, acquired and managed patients, provided facilities, etc.): K. De, T.M. Grubb, A.A. Zalenski, K.E. Pfaff, M.K. Summers, M. Venere
Analysis and interpretation of data (e.g., statistical analysis, biostatistics, computational analysis): K. De, T.M. Grubb, A.A. Zalenski, K.E. Pfaff, M.K. Summers, M. Venere
Writing, review, and/or revision of the manuscript: K. De, T.M. Grubb, A.A. Zalenski, K.E. Pfaff, D. Pal, S. Majumder, M.K. Summers, M. Venere
Administrative, technical, or material support (i.e., reporting or organizing data, constructing databases): K. De, T.M. Grubb, A.A. Zalenski, M. Venere
Study supervision: M. Venere

Acknowledgments

The authors thank Dr. Liwen Zhang of the Proteomics Shared Resource at The Ohio State Comprehensive Cancer Center and Dr. Belinda Willard of the Lerner Research Institute Mass Spectrometry Laboratory for Protein Sequencing at the Cleveland Clinic Foundation for sample processing and analysis. We also thank members of the Venere laboratory for insightful discussion and constructive comments on the article. This work was supported by a Research Scholar Grant, RSG-18-066-01-TBG, from the American Cancer Society, an Internal Research Program Grant from The Ohio State University Comprehensive Cancer Center, and The Ohio State University Comprehensive Cancer Center/Department of Radiation Oncology start-up funds (to M. Venere); the Heritage College of Osteopathic Medicine Medical Student Research Seed Funding (to K.E. Pfaff); and R01GM112895 and R01GM108743 (to M.K. Summers). The Fusion Lumos instrument from the Lerner Research Institute Mass Spectrometry Laboratory for Protein Sequencing at the Cleveland Clinic Foundation was purchased via an NIH shared instrument grant, 1S10OD023436–01. Research reported in the publication was supported by The Ohio State University Comprehensive Cancer Center and the NIH under grant number P30 CA016058.

The costs of publication of this article were defrayed in part by the payment of page charges. This article must therefore be hereby marked *advertisement* in accordance with 18 U.S.C. Section 1734 solely to indicate this fact.

Received December 24, 2018; revised March 7, 2019; accepted April 24, 2019; published first April 29, 2019.

References

1. Stupp R, Hegi ME, Mason WP, van den Bent MJ, Taphoorn MJ, Janzer RC, et al. Effects of radiotherapy with concomitant and adjuvant temozolomide versus radiotherapy alone on survival in glioblastoma in a randomised phase III study: 5-year analysis of the EORTC-NCIC trial. Lancet Oncol 2009;10:459–66.
2. Stupp R, Brada M, van den Bent MJ, Tonn JC, Pentheroudakis G, ESMO Guidelines Working Group. High-grade glioma: ESMO Clinical Practice Guidelines for diagnosis, treatment and follow-up. Ann Oncol 2014;25: iii93–101.
3. Chen J, Li Y, Yu TS, McKay RM, Burns DK, Kernie SG, et al. A restricted cell population propagates glioblastoma growth after chemotherapy. Nature 2012;488:522–6.
4. Bao S, Wu Q, McLendon RE, Hao Y, Shi Q, Hjelmeland AB, et al. Glioma stem cells promote radioresistance by preferential activation of the DNA damage response. Nature 2006;444: 756–60.
5. Lathia JD, Mack SC, Mulkearns-Hubert EE, Valentim CL, Rich JN. Cancer stem cells in glioblastoma. Genes Dev 2015;29:1203–17.
6. Venere M, Fine HA, Dirks PB, Rich JN. Cancer stem cells in gliomas: identifying and understanding the apex cell in cancer's hierarchy. Glia 2011;59:1148–54.
7. Lee AJ, Endesfelder D, Rowan AJ, Walther A, Birkbak NJ, Futreal PA, et al. Chromosomal instability confers intrinsic multidrug resistance. Cancer Res 2011;71:1858–70.

8. Li R, Hehlman R, Sachs R, Duesberg P. Chromosomal alterations cause the high rates and wide ranges of drug resistance in cancer cells. Cancer Genet Cytogenet 2005;163:44–56.
9. Godek KM, Venere M, Wu Q, Mills KD, Hickey WF, Rich JN, et al. Chromosomal instability affects the tumorigenicity of glioblastoma tumor-initiating cells. Cancer Discov 2016;6:532–45.
10. Sansregret L, Patterson JO, Dewhurst S, Lopez-Garcia C, Koch A, McGranahan N, et al. APC/C Dysfunction limits excessive cancer chromosomal instability. Cancer Discov 2017;7:218–33.
11. Wasch R, Robbins JA, Cross FR. The emerging role of APC/CCdh1 in controlling differentiation, genomic stability and tumor suppression. Oncogene 2010;29:1–10.
12. Garcia-Higuera I, Manchado E, Dubus P, Canamero M, Mendez J, Moreno S, et al. Genomic stability and tumour suppression by the APC/C cofactor Cdh1. Nat Cell Biol 2008;10:802–11.
13. Venere M, Horbinski C, Crish JF, Jin X, Vasanji A, Major J, et al. The mitotic kinesin KIF11 is a driver of invasion, proliferation, and self-renewal in glioblastoma. Sci Transl Med 2015;7:304ra143.
14. Mao DD, Gujar AD, Mahlokozera T, Chen I, Pan Y, Luo J, et al. A CDC20-APC/SOX2 signaling axis regulates human glioblastoma stem-like cells. Cell Rep 2015;11:1809–21.
15. Xie Q, Wu Q, Mack SC, Yang K, Kim L, Hubert CG, et al. CDC20 maintains tumor initiating cells. Oncotarget 2015;6:13241–54.
16. Schonberg DL, Miller TE, Wu Q, Flavahan WA, Das NK, Hale JS, et al. Preferential iron trafficking characterizes glioblastoma stem-like cells. Cancer Cell 2015;28:441–55.
17. Sackton KL, Dimova N, Zeng X, Tian W, Zhang M, Sackton TB, et al. Synergistic blockade of mitotic exit by two chemical inhibitors of the APC/C. Nature 2014;514:646–9.
18. Herzog F, Primorac I, Dube P, Lenart P, Sander B, Mechtler K, et al. Structure of the anaphase-promoting complex/cyclosome interacting with a mitotic checkpoint complex. Science 2009;323:1477–81.
19. Passmore LA, Booth CR, Vénien-Bryan C, Ludtke SJ, Fioretto C, Johnson LN, et al. Structural analysis of the anaphase-promoting complex reveals multiple active sites and insights into polyubiquitylation. Mol Cell 2005;20:855–66.
20. Yadav L, Tamene F, Göös H, van Drogen A, Katainen R, Aebersold R, et al. Systematic analysis of human protein phosphatase interactions and dynamics. Cell Syst 2017;4:430–44.
21. Keck JM, Summers MK, Tedesco D, Ekholm-Reed S, Chuang LC, Jackson PK, et al. Cyclin E overexpression impairs progression through mitosis by inhibiting APC(Cdh1). J Cell Biol 2007;178:371–85.
22. Eguren M, Alvarez-Fernandez M, Garcia F, Lopez-Contreras AJ, Fujimitsu K, Yaguchi H, et al. A synthetic lethal interaction between APC/C and topoisomerase poisons uncovered by proteomic screens. Cell Rep 2014;6:670–83.
23. Drosopoulos K, Tang C, Chao WC, Linardopoulos S. APC/C is an essential regulator of centrosome clustering. Nat Commun 2014;5:3686.
24. Yeong FM, Lim HH, Wang Y, Surana U. Early expressed Clb proteins allow accumulation of mitotic cyclin by inactivating proteolytic machinery during S phase. Mol Cell Biol 2001;21:5071–81.
25. Huang JN, Park I, Ellingson E, Littlepage LE, Pellman D. Activity of the APC (Cdh1) form of the anaphase-promoting complex persists until S phase and prevents the premature expression of Cdc20p. J Cell Biol 2001;154:85–94.
26. Amon A, Irniger S, Nasmyth K. Closing the cell cycle circle in yeast: G2 cyclin proteolysis initiated at mitosis persists until the activation of G1 cyclins in the next cycle. Cell 1994;77:1037–50.
27. Zachariae W, Schwab M, Nasmyth K, Seufert W. Control of cyclin ubiquitination by CDK-regulated binding of Hct1 to the anaphase promoting complex. Science 1998;282:1721–4.
28. Kramer ER, Scheuringer N, Podtelejnikov AV, Mann M, Peters JM. Mitotic regulation of the APC activator proteins CDC20 and CDH1. Mol Biol Cell 2000;11:1555–69.
29. Chang L, Zhang Z, Yang J, McLaughlin SH, Barford D. Atomic structure of the APC/C and its mechanism of protein ubiquitination. Nature 2015;522:450–4.
30. Miller JJ, Summers MK, Hansen DV, Nachury MV, Lehman NL, Loktev A, et al. Emi1 stably binds and inhibits the anaphase-promoting complex/cyclosome as a pseudosubstrate inhibitor. Genes Dev 2006;20:2410–20.
31. Verma R, Peters NR, D'Onofrio M, Tochtrop GP, Sakamoto KM, Varadan R, et al. Ubistatins inhibit proteasome-dependent degradation by binding the ubiquitin chain. Science 2004;306:117–20.
32. Zeng X, Sigoillot F, Gaur S, Choi S, Pfaff KL, Oh DC, et al. Pharmacologic inhibition of the anaphase-promoting complex induces a spindle checkpoint-dependent mitotic arrest in the absence of spindle damage. Cancer Cell 2010;18:382–95.
33. Lub S, Maes A, Maes K, De Veirman K, De Bruyne E, Menu E, et al. Inhibiting the anaphase promoting complex/cyclosome induces a metaphase arrest and cell death in multiple myeloma cells. Oncotarget 2016;7:4062–76.
34. Gao Y, Zhang B, Wang Y, Shang G. Cdc20 inhibitor apcin inhibits the growth and invasion of osteosarcoma cells. Oncol Rep 2018;40:841–8.
35. Lukas C, Sorensen CS, Kramer E, Santoni-Rugiu E, Lindeneg C, Peters JM, et al. Accumulation of cyclin B1 requires E2F and cyclin-A-dependent rearrangement of the anaphase-promoting complex. Nature 1999;401:815–8.
36. Listovsky T, Oren YS, Yudkovsky Y, Mahbubani HM, Weiss AM, Lebendiker M, et al. Mammalian Cdh1/Fzr mediates its own degradation. EMBO J 2004;23:1619–26.
37. Huang JN, Park I, Ellingson E, Littlepage LE, Pellman D. Activity of the APC (Cdh1) form of the anaphase-promoting complex persists until S phase and prevents the premature expression of Cdc20p. J Cell Biol 2001;154:85–94.
38. Jaspersen SL, Charles JF, Morgan DO. Inhibitory phosphorylation of the APC regulator Hct1 is controlled by the kinase Cdc28 and the phosphatase Cdc14. Curr Biol 1999;9:227–36.
39. Jaquenoud M, van Drogen F, Peter M. Cell cycle-dependent nuclear export of Cdh1p may contribute to the inactivation of APC/C(Cdh1). EMBO J 2002;21:6515–26.
40. Hockner S, Neumann-Arnold L, Seufert W. Dual control by Cdk1 phosphorylation of the budding yeast APC/C ubiquitin ligase activator Cdh1. Mol Biol Cell 2016;27:2198–212.
41. Zhou Y, Ching YP, Chun AC, Jin DY. Nuclear localization of the cell cycle regulator CDH1 and its regulation by phosphorylation. J Biol Chem 2003;278:12530–6.
42. Wan L, Chen M, Cao J, Dai X, Yin Q, Zhang J, et al. The APC/C E3 ligase complex activator FZR1 restricts BRAF oncogenic function. Cancer Discov 2017;7:424–41.
43. The I, Ruijtenberg S, Bouchet BP, Cristobal A, Prinsen MB, van Mourik T, et al. Rb and FZR1/Cdh1 determine CDK4/6-cyclin D requirement in C. elegans and human cancer cells. Nat Commun 2015;6:5906.
44. Lubanska D, Porter L. Revisiting CDK inhibitors for treatment of glioblastoma multiforme. Drugs R D 2017;17:255–63.
45. Cancer Genome Atlas Research Network. Comprehensive genomic characterization defines human glioblastoma genes and core pathways. Nature 2008;455:1061–8.
46. Brennan CW, Verhaak RG, McKenna A, Campos B, Noushmehr H, Salama SR, et al. The somatic genomic landscape of glioblastoma. Cell 2013;155:462–77.
47. Xie Q, Wu Q, Horbinski CM, Flavahan WA, Yang K, Zhou W, et al. Mitochondrial control by DRP1 in brain tumor initiating cells. Nat Neurosci 2015;18:501–10.
48. Veas-Perez de Tudela M, Maestre C, Delgado-Esteban M, Bolanos JP, Almeida A. Cdk5-mediated inhibition of APC/C-Cdh1 switches on the cyclin D1-Cdk4-pRb pathway causing aberrant S-phase entry of postmitotic neurons. Sci Rep 2015;5:18180.
49. Kernan J, Bonacci T, Emanuele MJ. Who guards the guardian? Mechanisms that restrain APC/C during the cell cycle. Biochim Biophys Acta Mol Cell Res 2018;1865:1924–33.
50. Cappell SD, Mark KG, Garbett D, Pack LR, Rape M, Meyer T. EMI1 switches from being a substrate to an inhibitor of APC/C(CDH1) to start the cell cycle. Nature 2018;558:313–7.
51. Cappell SD, Chung M, Jaimovich A, Spencer SL, Meyer T. Irreversible APC (Cdh1) inactivation underlies the point of no return for cell-cycle entry. Cell 2016;166:167–80.
52. Bassermann F, Frescas D, Guardavaccaro D, Busino L, Peschiaroli A, Pagano M. The Cdc14B-Cdh1-Plk1 axis controls the G2 DNA-damage-response checkpoint. Cell 2008;134:256–67.
53. Huang X, Summers MK, Pham V, Lill JR, Liu J, Lee G, et al. Deubiquitinase USP37 is activated by CDK2 to antagonize APC(CDH1) and promote S phase entry. Mol Cell 2011;42:511–23.

Published OnlineFirst April 29, 2019; DOI: 10.1158/1541-7786.MCR-18-1361

54. Marucci G, Morandi L, Magrini E, Farnedi A, Franceschi E, Miglio R, et al. Gene expression profiling in glioblastoma and immunohistochemical evaluation of IGFBP-2 and CDC20. Virchows Arch 2008;453:599–609.
55. Bie L, Zhao G, Cheng P, Rondeau G, Porwollik S, Ju Y, et al. The accuracy of survival time prediction for patients with glioma is improved by measuring mitotic spindle checkpoint gene expression. PLoS One 2011;6:e25631.
56. Mao DD, Gujar AD, Mahlokozera T, Chen I, Pan Y, Luo J, et al. A CDC20-APC/SOX2 signaling axis regulates human glioblastoma stem-like cells. Cell Rep 2015;11:1809–21.
57. Ding Y, Yu S, Bao Z, Liu Y, Liang T. CDC20 with malignant progression and poor prognosis of astrocytoma revealed by analysis on gene expression. J Neurooncol 2017;133:87–95.

Published OnlineFirst April 29, 2019; DOI: 10.1158/1541-7786.MCR-18-1361

Molecular Cancer Research

Hyperphosphorylation of CDH1 in Glioblastoma Cancer Stem Cells Attenuates APC/C ^{CDH1} Activity and Pharmacologic Inhibition of APC/C $^{CDH1/CDC20}$ Compromises Viability

Kuntal De, Treg M. Grubb, Abigail A. Zalenski, et al.

Mol Cancer Res 2019;17:1519-1530. Published OnlineFirst April 29, 2019.